NDT&E International 84 (2016) 76–88

Contents lists available at ScienceDirect

NDT&E International

journal homepage: www.elsevier.com/locate/ndteint

Stress based non-destructive evaluation using thermographic approaches: From laboratory trials to on-site assessment

R.C. Tighe [a,*], G.P. Howell [a], J.P. Tyler [b], S. Lormor [c], J.M. Dulieu-Barton [a]

[a] University of Southampton, Southampton, UK
[b] Enabling Process Technologies, Portishead, UK
[c] Coal Stations Fleet, EDF Energy, West Burton, UK

ARTICLE INFO

Article history:
Received 4 May 2016
Received in revised form
24 August 2016
Accepted 30 August 2016
Available online 31 August 2016

Keywords:
Thermoelastic stress analysis
Stress assessment
Non-destructive evaluation
On-site application

ABSTRACT

Vibration based loading has been successfully used to facilitate out of laboratory inspections using thermoelastic stress analysis enabling stress based non-destructive assessment of structures. An initial plate study verified the technique. A laboratory demonstrator of the on-site implementation was created to facilitate the development and assessment of a suitable loading device. The developed system was then taken on-site at a coal fired power station during a scheduled outage period. Vibration loaded thermoelastic stress analysis was successfully applied to welds in high pressure steam drain lines in-situ.

1. Introduction

The most common techniques currently applied in non-destructive evaluation (NDE) in industry are generally ultrasound (UT) based approaches. Essentially, UT is a 'point-by-point' measurement technique so inspections of large areas can prove extremely time consuming [1]. In the power industry, as with many others, the most common procedure used for the identification of defects in welds is phased array UT [2]. The process for weld inspection and reporting is laborious involving comparison to a reference case and manual plotting of results. As such the time consuming nature of UT leads to the inspection of selected sites only. The results of thermoelastic stress analysis (TSA) form images hence there is no need to make drawings to estimate damage size rather the data may be directly assessed and stored. While UT may successfully locate and size defects it cannot provide directly any prognostic information on how the defect is affecting the structural performance. There is a clear case for an alternative on-site inspection technique to be used in a complementary manner with UT that can provide rapid inspections and prognostic information. TSA is a full-field thermographic technique which relates the thermal response of a component subjected to cyclic loading, within the elastic limits of the material, to the sum of the principal stresses [3]. TSA data can be captured in as little as 10 s. Perhaps more importantly, TSA provides visual information as a stress map which shows directly the redistribution of the stresses resulting from any defect enabling it to be used as both a diagnostic and, with some addition material property information, prognostic tool. Although TSA is a surface technique, sub surface damage will cause a redistribution of the stresses which, depending on the defect depth, will modify the thermoelastic response from the surface. The present paper focuses on the development of TSA as a new stress based NDE approach which could be used for standalone inspections or in conjunction with traditional NDE approaches.

The aim is to use TSA for the inspection and analysis of in situ in service components. Therefore an alternative means of loading has been devised based on exciting the component at its resonant frequency during data collection to generate sufficient stress to provide a measurable thermoelastic response. Some early work [4] used the Stress Pattern Analysis by Thermal Emissions (SPATE) system to identify delaminations in a fibre reinforced polymer composite cantilever beam. It was shown at 13.5 kHz the delamination caused a change in the thermoelastic response, but there were significant limitations imposed by SPATE system data capture rate. By the late 1990's detector capabilities had significantly improved enabling much higher thermal, spatial and temporal resolution. A study [5] using a more modern array based detector showed that a measureable thermoelastic response could be obtained from aluminium alloy, steel and polycarbonate beams up to the fourth mode of vibration. More recently, vibration-based

* Corresponding author.
E-mail address: R.C.Tighe@soton.ac.uk (R.C. Tighe).

http://dx.doi.org/10.1016/j.ndteint.2016.08.005
0963-8695/

excitation has been used on aircraft composite sandwich panel components to explore the possibility of using TSA as an NDE technique [6].

In the present paper a new approach is proposed for NDE of ferritic steel pipes using TSA, although it should be noted that the procedure is applicable to all metals. Firstly the underlying idea is demonstrated in the laboratory environment on clamped thin aluminium plates. The challenge of generating sufficient load for much stiffer components than previously studied is addressed through the design of a laboratory demonstrator that incorporates a thick walled pipe representative of that used in steam plant for electricity generation. A new means of excitation is devised to provide the necessary cyclic loading that does not require electrical power so it can be deployed on-site. Finally, a detailed account of the preparations for and the installation of the new system during a scheduled outage at EDF Energy's coal fired power station at West Burton, UK is provided. The system is used to inspect a number of steam lines welds and its viability is demonstrated for use in on site applications. It is shown that TSA can be used to obtain the stresses in the pipework and that TSA can be used as NDE system in the challenging environment of a coal-fired power station. The work represents an important advance in NDE assessment as the stresses in the component are evaluated directly without recourse to models. The work described in the paper provides the basis for developing a generic stress based NDE system that can be used in a wide range of service applications.

2. General considerations for TSA

TSA uses an infra-red (IR) detector to monitor the surface temperature changes of a cyclically loaded component, which are related to the sum of the principal stresses as follows [2]:

$$\frac{\Delta T}{T} = -K(\Delta\sigma_1 + \Delta\sigma_2) \tag{1}$$

where T is the surface temperature, ΔT is the temperature change caused by the thermoelastic effect, $\Delta\sigma_{1+}\ \Delta\sigma_2$ is the sum of the change in the principal stresses (generally referred to as the 'stress sum') and K is the thermoelastic constant of the component material.

$$K = \frac{\alpha}{\rho C_p} \tag{2}$$

where α is the coefficient of thermal expansion, ρ is the density of the material and C_p is the specific heat at constant pressure.

In the present paper a FLIR SC5000 IR system was used. The system incorporates a 256 × 320 InSb photon detector array with a pixel pitch of 30 × 30 μm, capable of recording at 383 Hz at full frame in the spectral range of 3–5 μm. The thermal sensitivity of the detector is 20 mK, which is reduced to approximately 4 mK with application of the lock-in processing used in TSA. Data was collected and processed using the manufacturer's software Altair and Altair LI. As an example typical values of T and ΔT when testing at room temperature are room temperature (i.e. around 293 K) and of the order of 50 mK respectively.

In TSA the lock-in processing uses a 'reference signal' from the loading system to correlate the IR detector response and the applied stress [3]. Hence, both ΔT and T are provided, so the change in the sum of the principal stresses is obtained as per Eq. (1). If isentropic conditions prevail in the specimen the thermoelastic response, ΔT, occurs in-phase (compression) or 180° out-of-phase (tension) with the stress change. Deviation from isentropic conditions results in an out-of-phase response indicating that Eq. (1) is not valid. Therefore the phase data is a very useful and straightforward means of validation, as it is obtained alongside ΔT and T from the lock-in processing.

Typically the cyclic loading necessary to facilitate TSA is imparted using a servo-hydraulic test machine. The reference signal for the lock-in is obtained from the test machine load cell. This tethers TSA to a laboratory environment and hence a different means of imparting the load is required. It is proposed that a vibration based excitation at the component natural frequency could be used to generate the thermoelastic response. Natural frequency excitations have the potential to be much higher frequencies than typically studied with TSA therefore appropriate integration time (IT) [7] and frame rate must be selected. IT is akin to exposure time in photography, i.e. a short IT must be used to collect data from a fast moving scene to avoid blurring. However, a shorter integration time means fewer photons impinge on the detector resulting in a lower detector response. There is a trade-off between noise content and image quality, when selecting an appropriate IT. The frame rate should obey the Nyquist-Shannon criterion relative to the loading frequency. A further consideration is the source of the reference signal to perform the lock-in. There are several possibilities including force transducers, accelerometers as well as self-referencing where the collected IR data is used as the reference source. A range of reference signals were trialled and are discussed alongside each experiment in the following sections of the paper.

In all thermographic assessments there is a requirement to observe a surface of high and uniform emissivity; this is typically achieved through application of a thin layer of matt black spray paint. Substantial previous work has been carried out on selection of paint for the purposes of IR thermography. In most TSA studies RS matt black spray paint from RS Components has been used and a detailed characterisation was carried out in [8]. It has recently emerged that a change in the formula of RS matt black has occurred, reducing the adhesion to the surface of components and providing a significantly lower emissivity, which renders it unsuitable for quantitative TSA studies. To find a suitable replacement, a number of readily available alternative black paints were tested for surface finish and adhesion. From this down select the most suitable paint was identified as Electrolube EMBP400 matt black. To evaluate and compare the response of the Electrolube paint the thermoelastic constant of steel was determined and compared to an identical specimen coated with the original RS matt black paint. The test specimens were 40 × 3 mm in cross sectional area. A cyclic load of 6 ± 5 kN was applied to the specimens with a loading frequency of 10 Hz. Table 1 shows the calculated thermoelastic constant for the steel using both paints. To compare the results from the specimens with the new paint with

Table 1
Alternative paint study results.

Paint	Adhesion	Surface finish	Thermoelastic constant (Pa^{-1})	Normalised thermoelastic constant
Electrolube EMBP400 Matt Black	Very good adhesion to metal substrate. Sprayed in a fine mist	Smooth, even surface finish	3.62×10^{-12}	0.978
New formula RS Matt Black	Good adhesion, sprayed in a fine mist	Reflective and showed surface textures	4.03×10^{-12}	1.087

the response obtained from specimens coated with the original RS matt black paint used in [8], is presented in Table 1 as 'normalised' values. Normalised values were obtained by dividing the thermoelastic constant from the specimens with the new paint by the thermoelastic constant obtained using the original paint. The normalised values highlight the variation between the new paints and original paint. The Electrolube EMBP400 matt black provided the closest match in response to the original RS matt black paint and hence was selected for the work described in the present paper.

3. Laboratory trials

The purpose of the initial work is to assess the current detector system and loading approach using a simple set up with well-defined natural frequencies. Hence a fully clamped aluminium alloy plate was selected and excited in it first and second modes. The experimental setup is shown in Fig. 1. A 0.9 mm thick aluminium plate was positioned in a clamp to model 'built-in' boundary conditions to give in-plane plate dimensions of 330×203 mm. The clamp uses two steel frames either side of the plate and fastened together using 20 bolts torqued to 27 Nm to provide uniform clamping pressure around the edges of the plate.

The plate was excited using a LDS V201 permanent magnetic shaker from Brüel & Kjær which provided a sine peak force of 17.8 N and had a usable frequency range of 5–13,000 Hz. The shaker was attached to the plate via a rigid stinger, which was connected using a thin layer of beeswax. The beeswax provided sufficient adhesion for the stinger to remain attached to the plate during loading but allowed the shaker to be easily repositioned. A force transducer positioned between the shaker and stinger provided the reference signal for the TSA. The standoff distance between detector and plate was 0.75 m so that the whole plate was captured in a single image. The stinger was located at the expected peak of displacement for the second mode as it was possible to excite both first and second mode from this position.

To select appropriate experimental parameters such as IT and frame rate, it was necessary to establish the natural frequencies of the plate. Finite element analysis (FEA) was conducted using ANSYS 14.0 using SOLID185 elements with an element size of 0.9 mm. Modal analysis was undertaken, which provided the frequencies necessary to excite the first two modes for the aluminium plate assuming zero displacement at the clamped edges. The first and second modes, shown in Fig. 2, were given by the FEA with natural frequencies of 144 Hz and 209 Hz.

It was necessary to use the full frame of the detector to maximise spatial resolution so the detector was set to record at its maximum full frame rate of 383 Hz. This was suitable for the first mode but for the second mode the data capture falls just below the Nyquist-Shannon sampling criteria. However, as the lock-in processing is based on the reference signal and because data is recorded over several cycles, the lower relative frame rate is not a concern. Based on the predicted natural frequencies an IT of 700 μs was used.

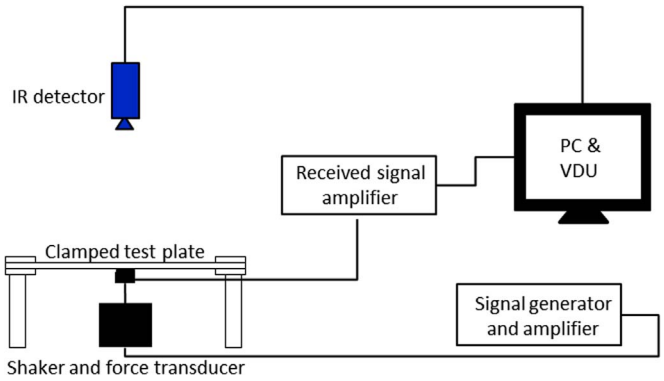

Fig. 1. Schematic of setup for clamped plate experiments.

During the experiments the predicted modal frequencies were tuned around to establish the exact frequency to account for the actual experimental conditions, such as clamping pressure and stinger connection, which were not included in the model. The experimentally determined first and second modal frequencies were 144 and 221 Hz respectively.

3.1. Laboratory trial results

The TSA results from the aluminium plate excited in its first and second mode are shown in Fig. 3. The results displayed are the $\Delta T/T$ data in Fig. 3a and d, which is directly related to the sum of the principal stresses. Fig. 3b and e show the $\Delta T/T$ profiles taken across the centre of the plates. Fig. 3c and f show the phase data which shows isentropic conditions are prevailing with the nodes clearly marking the change between an in-phase and an 180° out-of-phase response.

In Fig. 3a the effect of the stinger is apparent with a large concentration in $\Delta T/T$ data with the line plot shown in Fig. 3b emphasising the asymmetry around the stinger location. Aside from this bias, the TSA data shows the expected pattern for the excitation of the first mode in a clamped plate. The phase data shown in Fig. 3c reveals that the central region of the plate has a uniform phase but is out of phase with the outer region as expected as the response varies at the clamped edges. The stinger location is also evident in the phase data.

The results for the second mode on the aluminium plate are given in Fig. 3d–f. The second mode is clearly identified in the TSA $\Delta T/T$ data, but as with the first mode the presence of the stinger has a clear effect on the response. The bias caused by the stinger position is evident in the line plot data shown in Fig. 3e, taken across the two peaks of the second mode. The peaks are expected to be of similar magnitude and shape but there is a notable difference. The phase data shown in Fig. 3f reveals the node showing the two halves of the plate are out of phase as expected as well as the effects of the clamped edges.

The plate example demonstrates that natural frequency vibration can be used to obtain the thermoelastic response in a robust and repeatable approach to inspect components without the requirement of a test machine and confirms the findings of [5,9]. The data obtained from the current experiments is an improvement over that shown in [5] largely attributable to the improvement of the spatial and temporal resolution of the detector.

4. Laboratory demonstrator on representative pipework

The overall aim is to carry out on site assessment on pipe work; as such the next stage of development was to test the approach on a representative component. Several offcut sections of the steam drain pipe were provided by EDF West Burton. The sections were the same age and grade as the pipes in use on the plant but were unused; hence they suffered corrosion due to aging but no wear. The presence of surface corrosion severely hampers the efficient transfer of heat from the component and thus prevents accurate TSA measurements. It was necessary to investigate the surface preparation required to remove corrosion to allow effective adhesion of the matt black paint. The exact metal type was unknown beyond the knowledge that it was ferritic steel so it was necessary to carry out experiments to determine the thermoelastic constant using TSA.

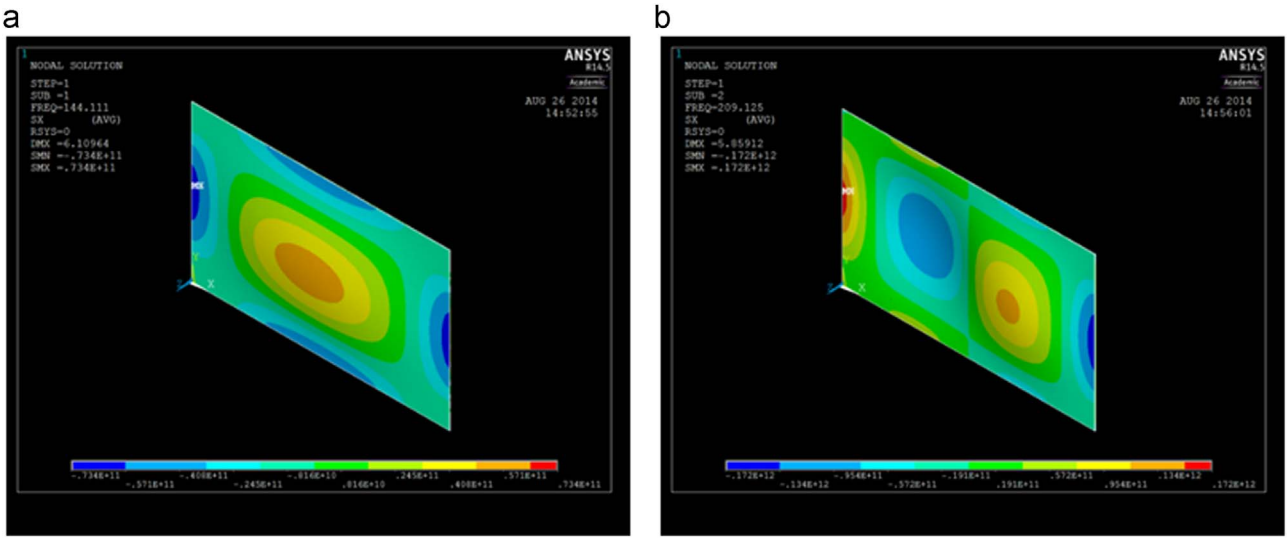

Fig. 2. FEA modal analysis results determining the frequencies of (a) mode 1 and (b) mode 2.

To establish the sensitivity of TSA to surface preparation prior to painting a 600 mm section of the steam drain pipe was used with outer diameter of 42 mm and wall thickness of 9 mm. Four levels of surface preparation were investigated. The first level (L1) used a wire brush to remove loose debris, the remaining three (L2-4) firstly used a wire brush and then used 80, 120 and 180 grit SiC paper respectively giving a progressively smoother finish. The pipe was then cyclically loaded in an Instron servo-hydraulic test machine in tension along the length of the pipe. The load applied was 99 ± 81 kN at a frequency of 10 Hz. $\Delta T/T$ values were obtained point by point and the average $\Delta T/T$ value was determined for each surface finish. Eq. (1) was then applied to give experimentally determined values of K as presented in Fig. 4, alongside their associated standard deviations shown by the error bars. The tests were repeated rotating the pipe 180° swapping the top and bottom ends to ensure there was no bias caused by pipe orientation or test machine grip alignment. Surface preparation level one was found to give a lower value of K with a much larger standard deviation than the remaining three levels where the SiC paper was used. Surface preparation levels L2-4 provide consistent measurements showing that the additional effort required to provide a smoother finish than that obtained with the 80 grit SiC paper was not necessary; however the wire brush alone is not a suitable surface preparation. All pipe inspections were therefore carried out with L2 surface preparation using the wire brush and 80 grit SiC paper as there was no discernible different between the response from L2-L4 and L2 required the least effort. An estimation of the K can be obtained for a general steel from the literature as 3.04×10^{-12} Pa^{-1} [10], shown in Fig. 4 as the dotted line. The average experimentally determined value of K found using the L2-4 data was 3.20×10^{-12} Pa^{-1} (shown in Fig. 4 as the solid line) which is within 6% of the estimated literature value of K, confirming the experimental approach to determine K is valid, particularly considering the actual grade of the ferritic steel is unknown. Therefore, the average experimentally determined value of K, i.e. 3.20×10^{-12} Pa^{-1}, was used to calculate the stress sum data in the remainder of the paper.

A second longer section of the pipe was provided that measured 1.513 m long, with outer diameter of 48.5 mm and wall thickness of 6.75 mm, was used for the laboratory based demonstrator. Two 10 mm thick EN3 steel end plates were TIG welded to both ends of the pipe section following guidelines for on-site welds, creating a single pass fillet weld. The pipe rig was rigidly fastened to a T-slot plate to ensure when excited only the pipe could move creating a fixed-fixed end test set-up. Based on the results of the Fig. 4 and Table 1 the pipe surface was prepared using preparation level 2 and spray painted matt black using the Electrolube EMB400 paint. Fig. 5a shows the prepared pipe surface at the end of the pipe compared to its as received state, the painted inspection area is shown in Fig. 5b.

Due to the increased stiffness of the pipe compared to the previously assessed plates it was necessary to determine a more suitable loading approach able to provide the required force and frequency excitation to the component. The pipe was excited in its first mode using two excitation approaches firstly a permanent magnetic shaker was used, a larger version than that in the plate studies, and then secondly a more portable pneumatic approach was used.

4.1. Demonstrator I – permanent magnetic shaker

The permanent magnetic shaker used for pipe excitation was a Ling V406 with a usable frequency range of 5–9000 Hz and a peak sine force of 98 N. The mass of the shaker when mounted on a trunnion was 22.7 kg and 14.1 kg without the trunnion. The shaker was attached to the pipe using a rigid stinger and beeswax as in the plate study. Instrumented hammer tests were undertaken and the transfer function was used to identify first natural frequency for the pipe as shown in Fig. 6. The first mode was found to be at 100 Hz. A signal generator was used to provide the required loading frequency, the experimental set up and corresponding schematic are shown in Fig. 7a and b. A force transducer positioned between the shaker and stinger was used to provide the reference signal for TSA. The shaker was positioned at the anti-node of the first mode, i.e. in the centre of the pipe. It is noted that the stinger was attached to the side of the pipe to allow both directions of movement to be captured.

4.2. Demonstrator II – pneumatic shaker

Due to the moderately large mass of the permanent magnetic shaker rendering it difficult to move and difficult attach to pipes on-site where access may be limited, a lighter and smaller solution was sought. A Vibtec GT36 pneumatic shaker was investigated as a possible means of excitation. The GT36 used a conventional workshop air supply to rotate a turbine wheel with an imbalance mass distribution to create a vibration excitation in an object to which it is rigidly clamped. The frequency and force of the loading

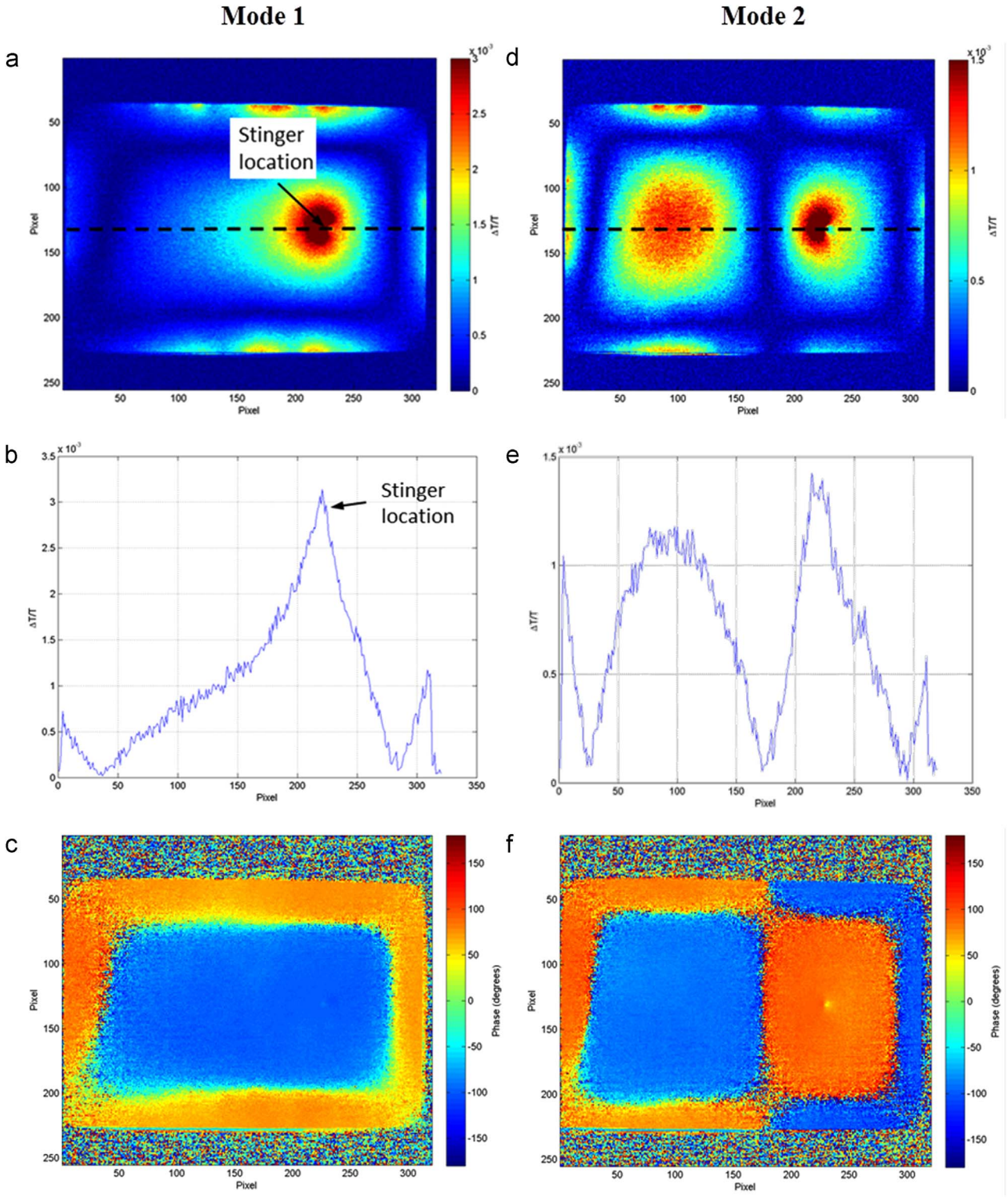

Fig. 3. TSA results of the aluminium clamped plate excited at mode one (a–c) and two (d–f) showing (a) mode one $\Delta T/T$ data, (b) $\Delta T/T$ profile plot taken along the dashed line in (a), (c) mode one phase data, (d) mode two $\Delta T/T$ data, (e) $\Delta T/T$ profile plot taken along the dashed line in (d), (f) mode two phase data.

is controlled by varying the air flow rate. The manufacturer's specification of the GT36 lists a frequency range of 100–250 Hz and a maximum force of 8 kN, however both force and frequency are greatly reduced when attaching the shaker to a less rigid structure such as the pipe. To attach the pneumatic shaker to the pipe, a clamping system, shown in Fig. 8, was custom built to accommodate a variation in pipe outer diameter between 35 and 50 mm. The clamp was such that it was securely gripped to the pipe to avoid detachment during testing and avoid damping of the vibration loading. The mass of the pneumatic shaker is 2.3 kg and the mass of the shaker with the clamping system is 5 kg thus reducing the total mass to less than a third of the permanent magnetic shaker. The experimental setup is shown in Fig. 8a and schematic in Fig. 8b. The shaker uses a workshop air line, a filter and valve is fitted between the air line connection and the shaker to allow easy pressure control and filtration. The shaker and clamp

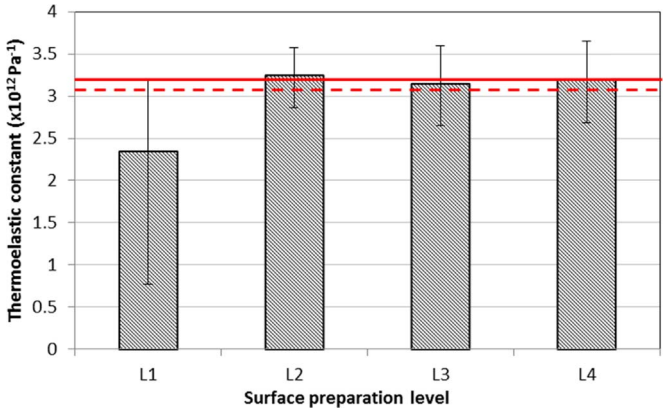

Fig. 4. Experimentally determined *K* values comparing surface finishes L1-4. With literature value (dashed line) and the mean experimental value taken from L2-4 (solid line).

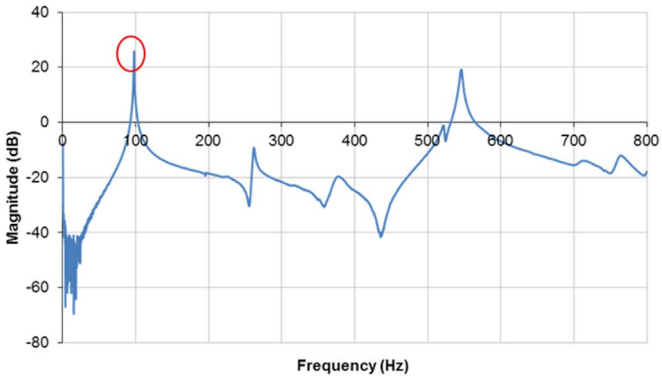

Fig. 6. Transfer function used to identify the first mode excitation frequency for the permanent magnetic shaker.

are bolted to the centre of the pipe. The data is collected as in demonstrator I. In this set-up it is difficult and impractical in the context of an on-site application to obtain a reference signal from an accelerometer, because of interference from other systems. Therefore, it was decided to use a self-referencing lock-in approach to process the thermal data. The approach involves establishing the mean temperature over an area of pixels from the surface of the component through time. This data is then processed using a fast Fourier transform (FFT) to extract the frequency spectra so that the component with the largest amplitude is used as the reference signal. This approach differs to that found in [11], which deals with transient loading and utilises a least squares approach directly using the thermographic data as a reference signal. The approach in [11] cannot be used to obtain stresses but only give an indication of stress hotspots as it uses the temperature data itself as the reference signal and hence produces a relative rather than absolute stress map. The approach used in this paper uses the thermography data to determine a frequency reference signal, hence stresses can be derived. To establish the reference frequency it was found that using the response from close to the location of the maximum stress concentration provided a clear maximum in the frequency spectra obtained from the FFT. It should be noted that with the self-referencing approach some trial and error is required to identify the correct reference frequency, in general it was found that areas with low thermoelastic response, where noise dominates, did not provide an accurate reference frequency.

As the pneumatic shaker is clamped on the pipe the added mass of shaker must be taken into account when finding the natural frequency of the pipe set-up. Instrumented hammer tests were repeated with shaker attached and the first natural frequency was found to be 61.5 Hz with the shaker added mass.

4.3. Demonstrator results

The pipe was excited at 100 Hz for demonstrator I and 42.2 Hz for demonstrator II. Whereas demonstrator I has an electronic control of the exact excitation frequency demonstrator II is dependent on the air flow as well as the clamping conditions and the structure it is connected to and as such the frequency achieved in demonstrator II was below the desired natural frequency of 61.5 Hz, nevertheless a good thermoelastic response was obtained.

The $\Delta T/T$ and phase results for demonstrator I are given in Fig. 9a and b. Demonstrator I $\Delta T/T$ results show stress concentrations occur at the sides of the weld under cyclic loading with a line of zero stress along to top of the pipe. These stress

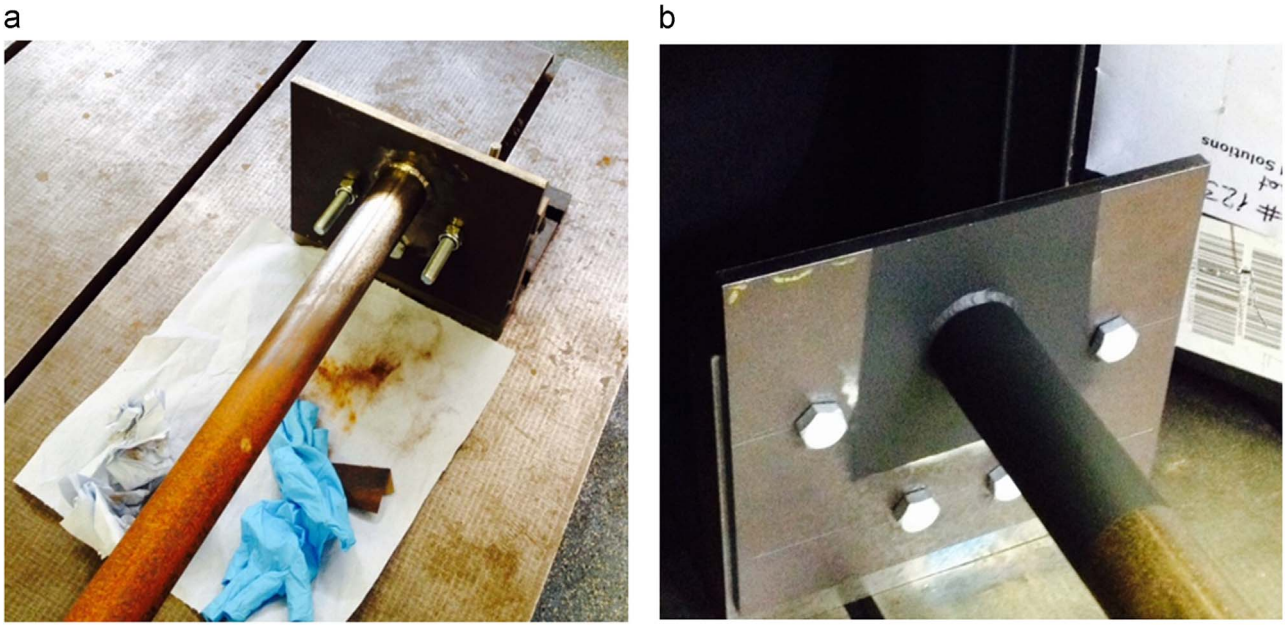

Fig. 5. Pipe surface preparation for TSA inspections (a) corrosion removal and (b) matt black spray painted inspection area.

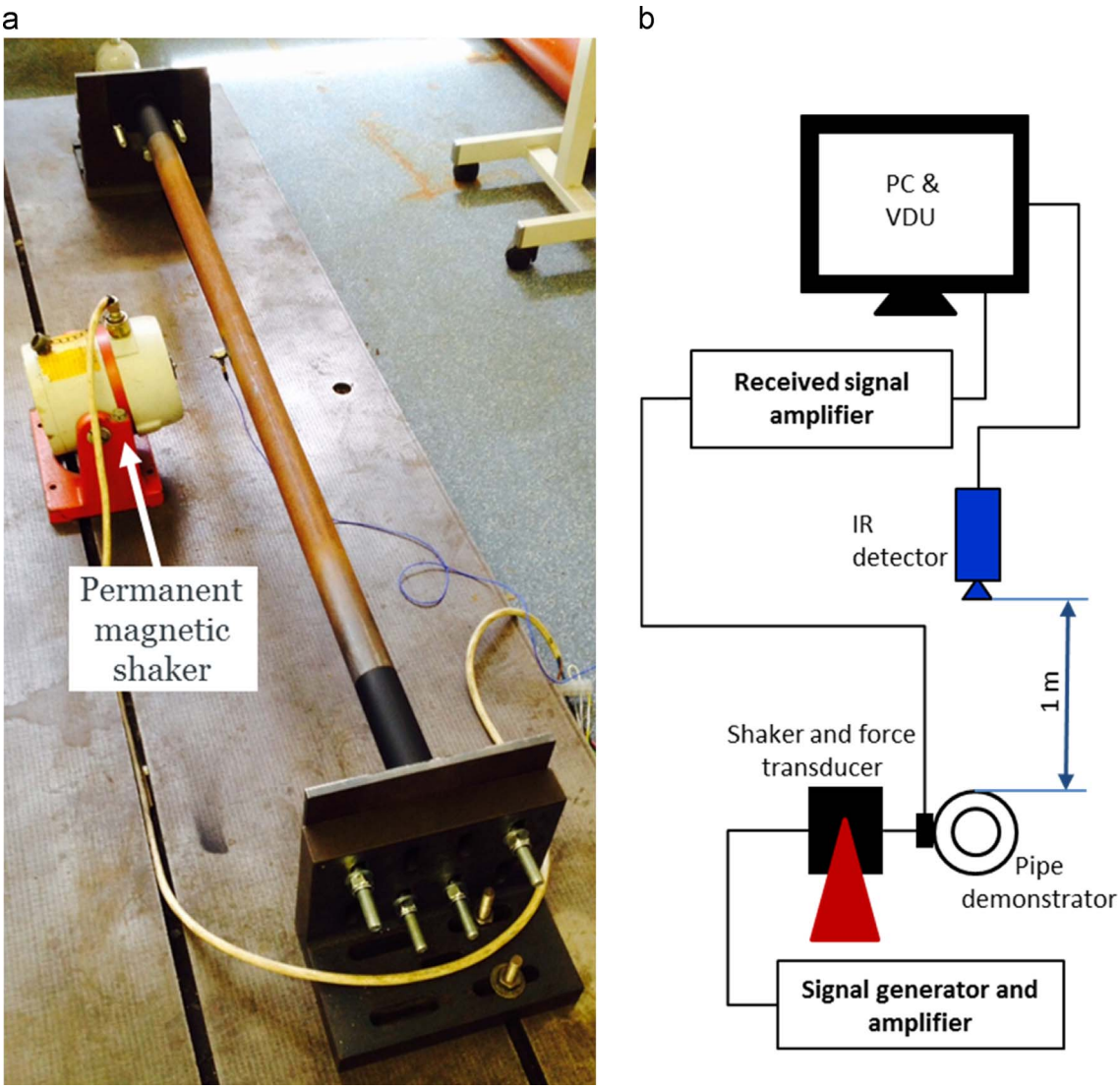

Fig. 7. Demonstrator I (a) photograph of shaker positioning and (b) schematic of full experimental set up.

distributions are caused by the orientation of the loading direction which, as shown in Fig. 7a is from the side of the pipe. The peak tensile and compressive stresses are clearly shown where expected at the weld and the line of zero stress corresponds to the neutral plane in this loading configuration. The selections of detector position and shaker orientation are important as this governs what is observed in the TSA data. In many cases it would be necessary to collect data from multiple observation angles to enable full inspection of a component, for example, of a girth weld. The shaker orientation determines the loading and hence the stress distribution. Clearly in areas where the stress is zero any defects would not be detected. Simply changing the shaker position or excitation frequency alters the stress field to reveal the defect. For example, in the demonstrator moving the shaker so that the excitation is in the vertical instead of the horizontal direction changes the neutral plane of the pipe. The phase data is 180° apart clearly highlighting the location of the neutral plane and indicating regions of tensile and compressive stress.

A comparison of the TSA data obtained for demonstrator I processed using the force transducer reference signal and the self-reference approach has been undertaken. The stress sum, as given by Eq. (1), was derived for both approaches along the profile line in Fig. 9 and is shown in Fig. 10a. $\Delta T/T$ data was extracted along each line and converted into the sum of the principal stresses using the experimentally determined K value of 3.20×10^{-12} Pa^{-1}. Fig. 10a shows that the two data sets are practically identical; to examine the difference the self-referenced data was normalised against the transducer lock-in data as shown in Fig. 10b. The greatest differences between the two approaches are found where the stresses are very low. The areas of higher stresses are in good agreement with less than 4% difference between the two approaches between pixels 30 and 45. The maximum stress sum is 52.6 MPa for both cases, hence the self-referencing lock-in approach is validated and can be used in future tests.

Demonstrator II results are given in Fig. 11a and b. Fig. 11a shows the stress distribution in the pipe generated in Demonstrator II; the stress concentrations around the weld are clear. The main difference between the results from demonstrator I and II is that in II the neutral plane is not clearly defined along the centre of the pipe. This is because the pneumatic shaker creates a slightly elliptical motion which modifies the stresses. Also the excitation frequency is below the natural frequency, hence the amplitude of deflection is lower, reducing the magnitude of the stresses. Despite this the stress distribution shown highlights the same stress concentrations as demonstrator I. The phase data shown in Fig. 11b also highlights the slightly elliptical nature of the pneumatic excitation where the neutral plane is not as clearly defined as with demonstrator I.

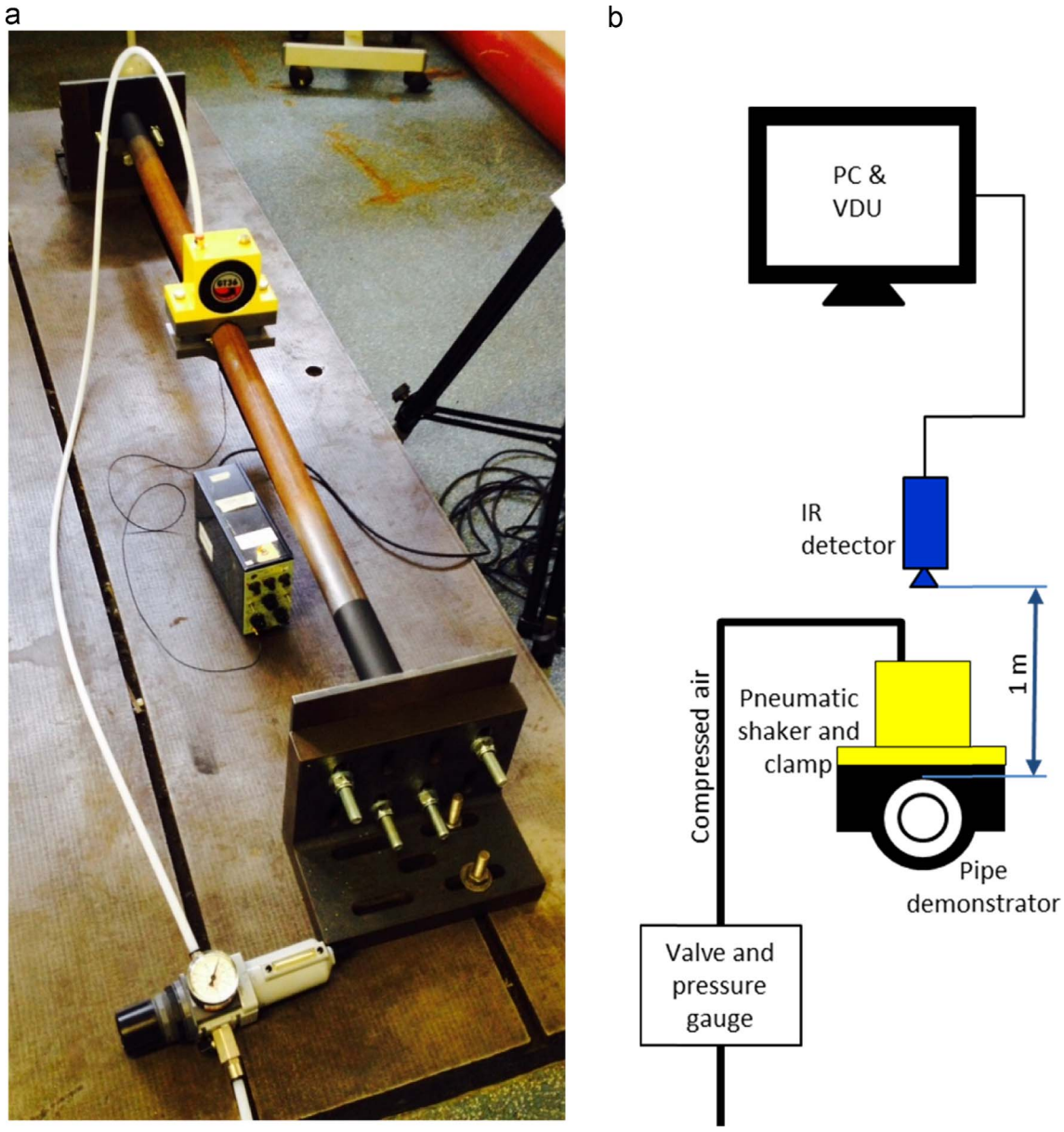

Fig. 8. Demonstrator II (a) photograph of pneumatic shaker positioning and (b) schematic of full experimental set up.

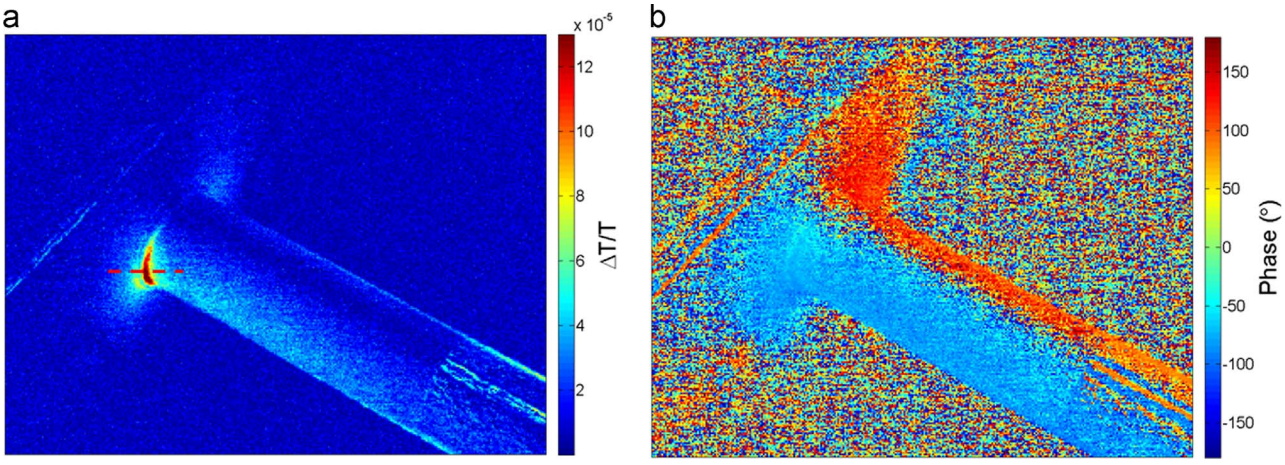

Fig. 9. (a) TSA $\Delta T/T$ and (b) phase results for demonstrator I.

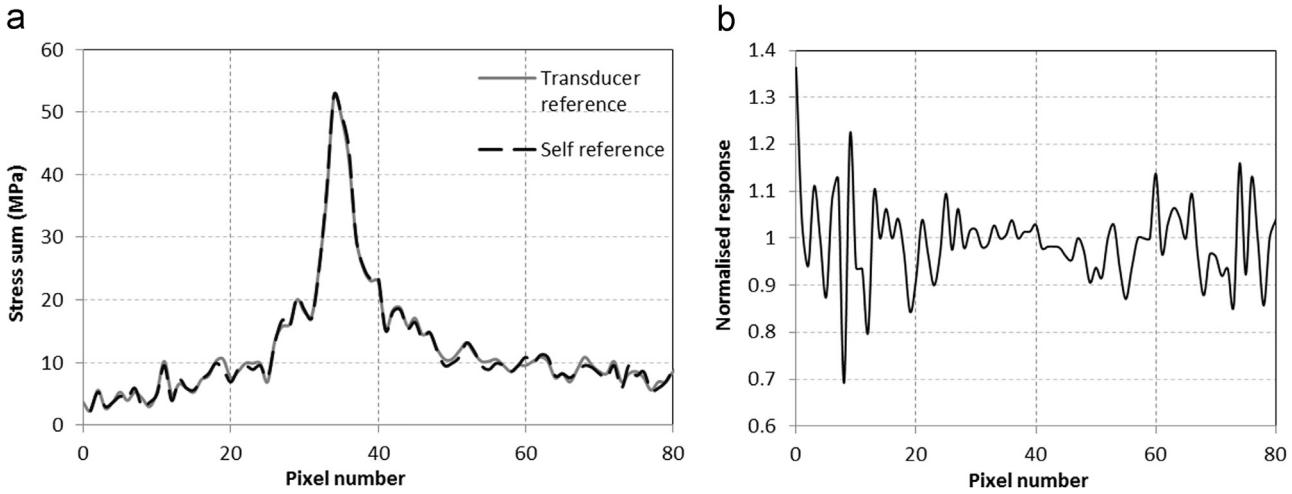

Fig. 10. (a) Stress sum profile data using the force transducer and self-reference signals and (b) self-referenced stress sum data normalised against transducer reference data.

Fig. 12 shows line plots of stress sum from both demonstrators along the lines indicated in Figs. 9a and 11a. The $\Delta T/T$ data was converted into the sum of the principal stresses to enable a direct comparison of the stresses obtained for both loading approaches. The peak stress sum for demonstrators I and II are 53 MPa and 41 MPa respectively, i.e. well below the yield strength of steel (which is >200 MPa for even the lowest grade steel). Fig. 12 shows that although the peak stress is higher in demonstrator I, which is as expected as the system is vibrating at its natural frequency, the stress in the pipe is larger in demonstrator II resulting from a change in the stresses caused by the excitation of the pneumatic shaker.

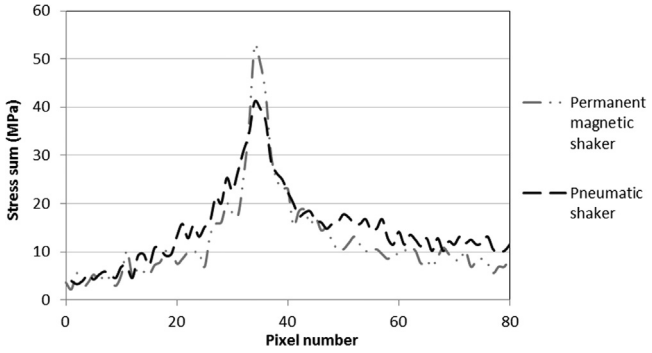

Fig. 12. Stress sum profiles taken across the weld for demonstrators I and II.

5. On-site assessment

As both demonstrators had functioned well in laboratory based conditions the next stage was to take a demonstrator on-site for pipe weld inspection using TSA. Due to the portability of the pneumatic shaker, only this was used on-site. Pipes were identified for inspection, as shown in Fig. 13, to provide a range of welds to consider. Pipe 1 had an outer diameter 48 mm and was multi-pass fillet welded to a larger section of pipe creating a T-junction similar to that found in the demonstrator study; this is designated weld 1.1 (see Fig. 14a). A series of three butt welds were located along the length of pipe 1, numbered as welds 1.2–1.4 in Fig. 14a. Pipe 1 had a 600 mm horizontal pipe run followed by a 90° bend to make a vertical 3 m pipe run. Welds 1.1 and 1.2 located on the horizontal section of pipe 1 are shown in Fig. 14b. Pipe 2 was a long straight section of pipe of outer diameter 43.5 mm with a single weld in the central region. The pipe length between supports was approximately 8 m.

It was necessary to prepare the surfaces of the inspection areas as in the laboratory. Pipe 1 was newly fitted so contained little corrosion, thus only a light sanding with the 80 grit SiC paper was required. Pipe 2 was 10 s of years old and had heavy surface corrosion that would seriously impede the TSA inspection. The weld on pipe 2 was cleaned using a battery powered grinder with an 80

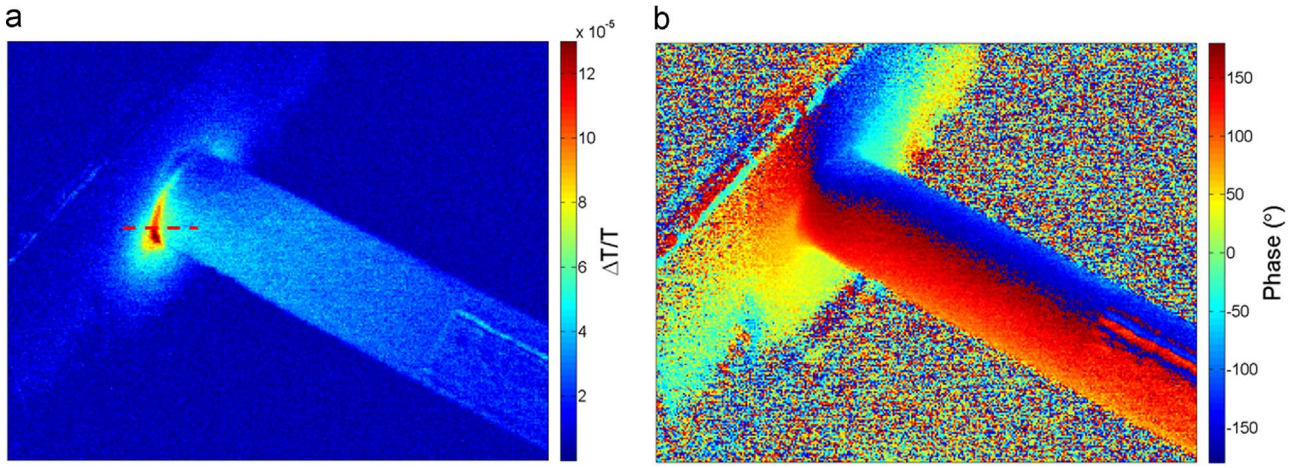

Fig. 11. (a) TSA $\Delta T/T$ and (b) phase results for demonstrator II.

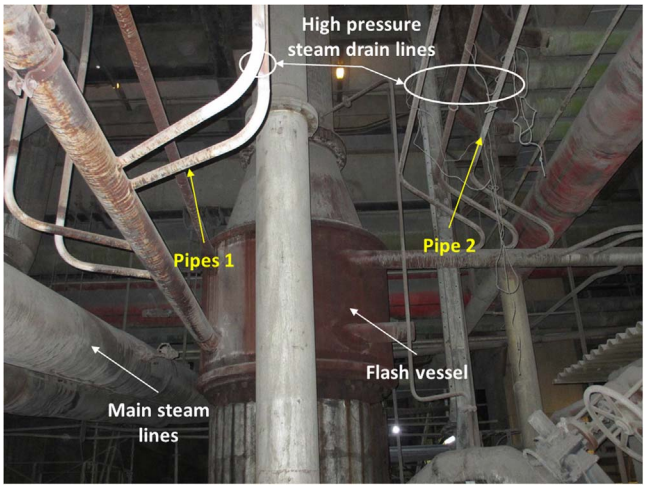

Fig. 13. Overview of inspection area at EDF West Burton.

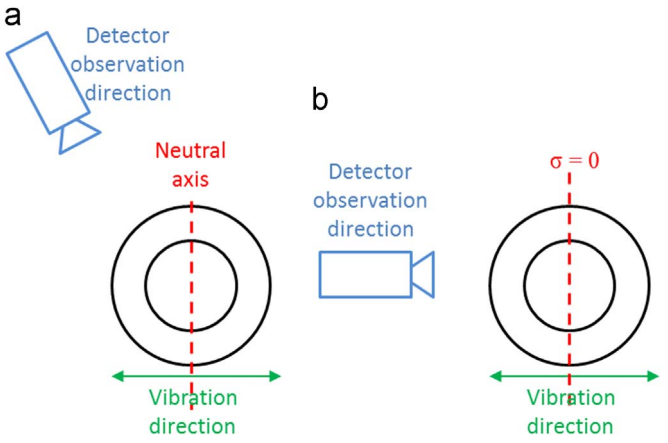

Fig. 15. Observation orientation of detector relative to primary vibration direction for (a) welds 1.1 and 1.2 and (b) welds 1.3 and 1.4.

grit flapper wheel, taking around 3–5 min. The surface was then cleaned with a cloth and acetone to remove any remaining dirt or grease. (It should be noted that this surface preparation would be necessary before applying other inspection techniques, including ultrasound). A thin layer of the Electrolube matt black spray paint was then applied. Due to the time restrictions for work on-site the shaker was positioned at a single site on each pipe to inspect all the welds along that pipe. The shaker position for pipe 1 is shown in Fig. 14 located at the midpoint of horizontal section of the pipe. The shaker was operated using a constant air pressure of 1.5 bar for all weld inspections. The excitation frequency was then determined using the self-reference lock-in processing as previously described. The areas selected for determining the reference frequencies were local to the inspection sites to ensure that the frequency of the local vibration was used for processing.

The detector observation orientation must be considered when assessing the results as this controls what is visible in the images. It is important to note that the observation angles of the regions of interest in the pipes were also governed by the optical accessibility. For welds 1.1 and 1.2 the detector was orientated at around 45° relative to the vibration direction, as shown in Fig. 15a, whereas for welds 1.3 and 1.4 the detector was orientated parallel to the vibration direction, as in Fig. 15b.

5.1. On-site results

The $\Delta T/T$ data and phase data for welds 1.1–1.4 along pipe 1 are presented in Fig. 16. It should be noted that the scales on each image are different, with the intention to reveal as much information as possible. Weld 1.1 is the multi-pass fillet weld and stress concentrations are located at the sides of the weld as found with laboratory demonstrator. However, unlike demonstrator II the neutral plane is clear with a line of zero response evident along the top of the pipe. The elliptical movement of the pipe seen in the demonstrator is constrained by the pipe bend thus the dominant displacement is in the horizontal direction. The response for welds 1.3.and 1.4 is much less than 1.1 and 1.2 and the line of zero response is not clear. Also due to the observation direction with respect to the vibration direction the change in phase is less evident in the images from welds 1.3 and 1.4.

While in weld 1.1 the highest levels of stress are found at the edges of the weld material in weld 1.2 a stress concentration either side of the weld in the lower edge of the image is found. Similar stress concentrations are found at welds 1.3 and 1.4 also however to an apparent lesser effect. The effect of motion is much more evident in the data for welds 1.3 and 1.4 which manifests itself in the data at the edges outlining the pipe in the $\Delta T/T$ data. During testing it was noted that the upright pipe vibrated with higher

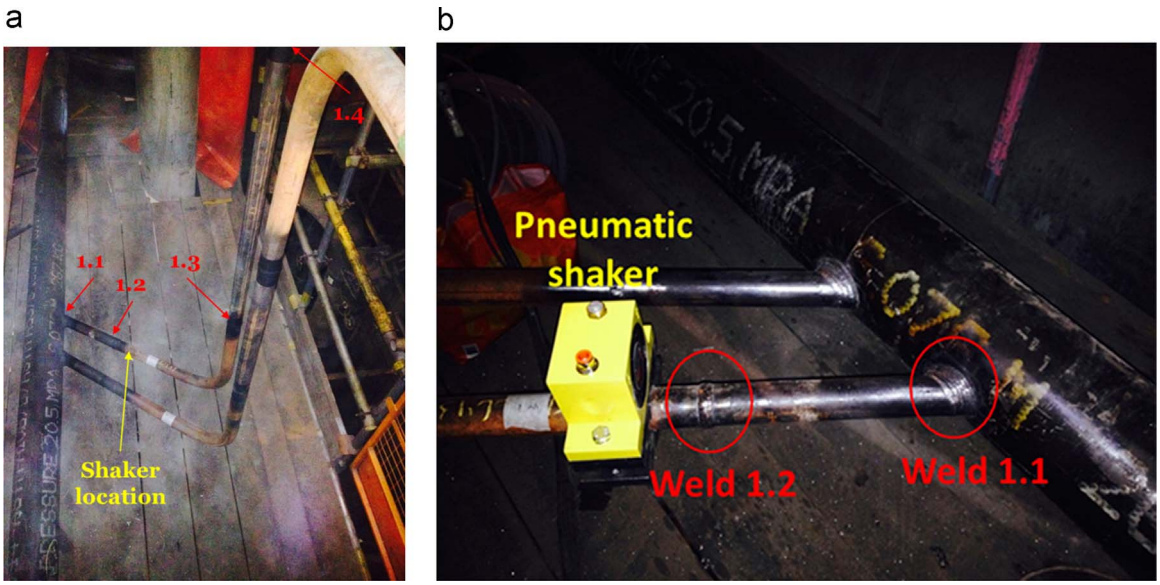

Fig. 14. (a) Weld and shaker locations highlighted on pipe 1, (b) shaker position on pipe 1 with welds 1.1 and 1.2 highlighted.

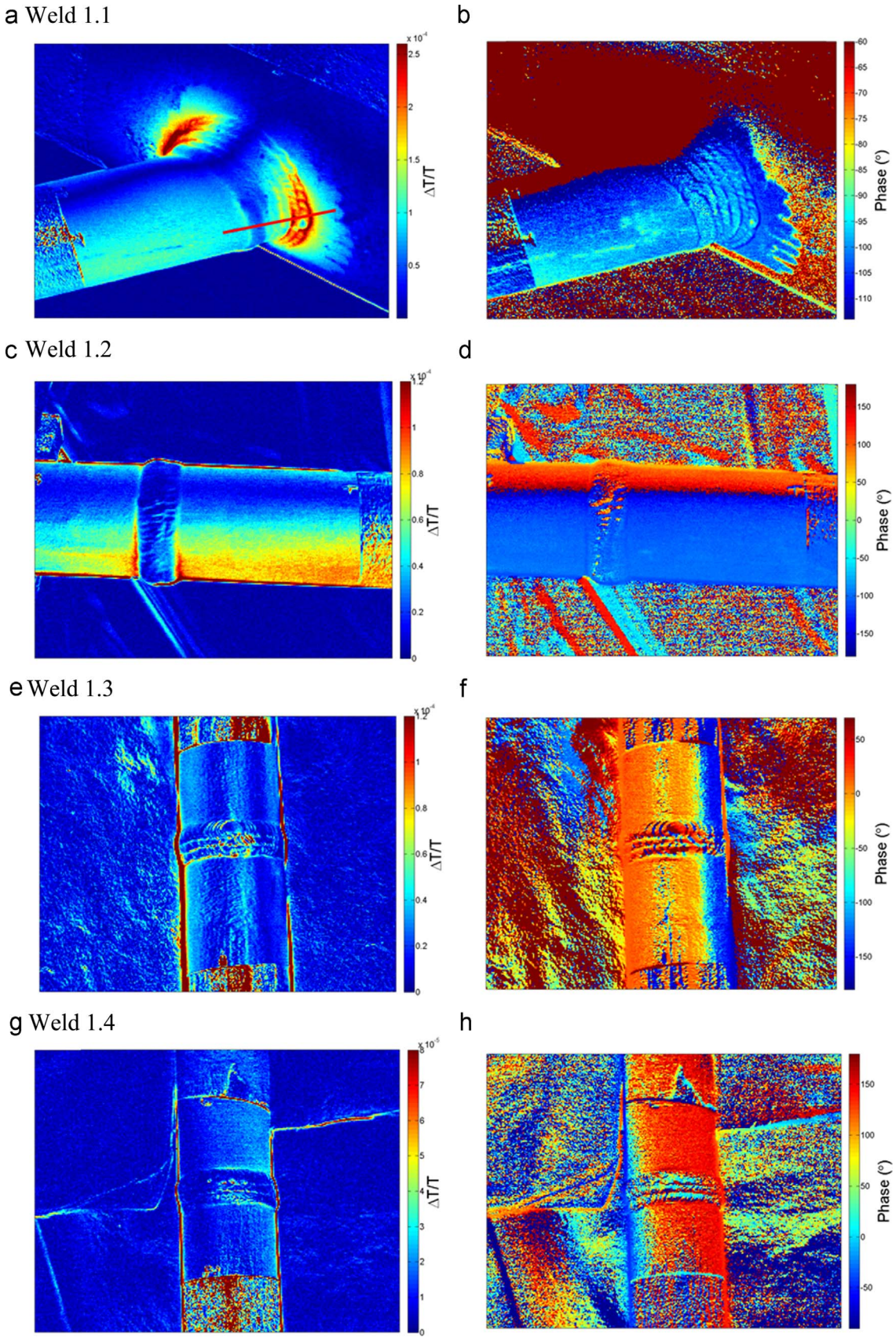

Fig. 16. TSA $\Delta T/T$ and phase results for welds 1.1–1.4 on pipe 1.

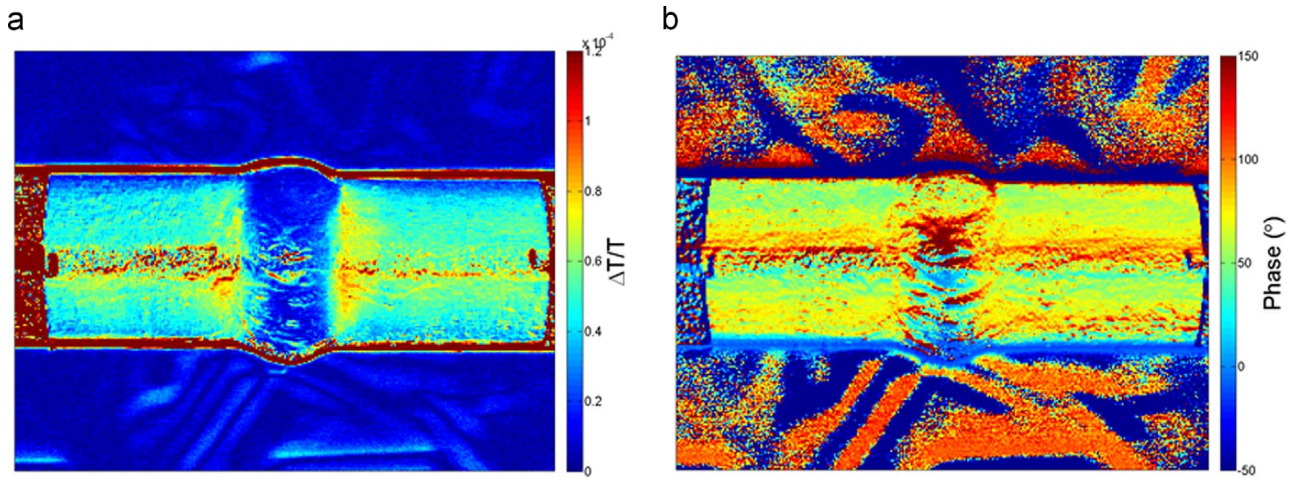

Fig. 17. TSA (a) $\Delta T/T$ and (b) phase results for weld 2.1 on pipe 2.

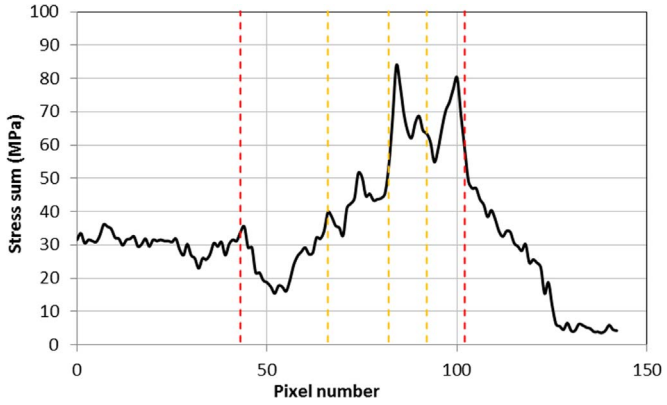

Fig. 18. Weld 1.1 stress sum data calculated along the profile line in Fig. 16a with weldment edges (red dashed line) and position of each weld pass (orange dashed line) marked. (For interpretation of the references to color in this figure legend, the reader is referred to the web version of this article).

amplitude than the shorter horizontal section. The effect of motion is also apparent in the phase data for these welds as the increased noise present in the data.

The $\Delta T/T$ and phase data for pipe 2 is presented in Fig. 17. As pipe 2 only contained a single weld towards the centre of the unsupported span on pipe the effect of motion is much more evident in the $\Delta T/T$ data. Nevertheless an area of increased response is apparent either side of the weld. There also appears to be noise in the data along a horizontal line which is caused by reflections and motion.

The maximum stress concentration that the pipe is experiencing is found at weld 1.1 where the pipe joins a larger section of pipe. A profile of the $\Delta T/T$ data is taken across the weld, as shown in Fig. 16a. Using the K value for the pipe material experimentally determined in Section 4, it is possible to calculate the sum of the principal stresses in the weld as plotted in Fig. 18. The edges of the weldment are marked on the graph as are approximate locations of the edges of each weld pass. The maximum stress sum created during TSA inspection is 84 MPa, again well below the material yield strength. Although initially there is a reduction in stress in the first weld pass at the smaller pipe end there is a general increase in magnitude of the stress sum within the weld moving from the smaller to the larger pipe. There are several peaks in the stress sum data across the width of the weld which appear to correlate with the weld passes although an additional peak is present at around pixel 75.

6. Conclusions

For the first time it has been shown that TSA can be successfully applied to components on-site in a challenging environment. To achieve this, the methodology was established through a small scale laboratory test followed by larger scale laboratory demonstrators representative of on-site application before finally taking the procedure on-site. On-site application of vibration loaded TSA using a pneumatic shaker was successful and yielded comparable results to those gathered using the laboratory demonstrator.

The work has shown that quantitative stress data can be obtained in regions where the motion was small. Motion prevented a quantitative analysis of the data sets, particularly when inspecting the parts of the steam pipe system away from any ‘fixed’ point. Further analysis is required to eliminate the effects of motion and is the object of current work.

The results clearly demonstrate the feasibility of using TSA as an on-site assessment approach. Further refinement is required and the next stage of work will involve the identification of known defects in welded samples to characterise the thermoelastic response from a range of typical defects present in welded joints. The present work uses a costly but highly sensitive photon detector, which makes it unattractive to industry, less expensive and more robust bolometers are presently being investigated which would be well suited to the application of TSA as a NDE approach.

Acknowledgements

The present work is part of an Innovate UK sponsored collaborative project under the “Developing the civil nuclear power supply chain” call, number 101438, Residual Stress and Structural Integrity Studies using Thermography (RESIST). Project partners include Enabling Process Technologies Ltd, University of Southampton, National Physical Laboratory, TWI, EDF Energy and Amec Foster Wheeler. We would also like to thank Dr Neil Ferguson at the University of Southampton for his help and support.

References

[1] Moles M. Phased arrays for general weld inspections. Olympus NDT, ⟨www.ndt.net⟩; 2010.
[2] Erhard A, Schenk G, Hauser T, Volz U. New applications using phased array techniques. Nucl Eng Des 2001;206:325–36.
[3] Dulieu-Barton JM. Thermoelastic stress analysis. In: Rastogi P, Hack E, editors. Optical methods for solid mechanics: a full-field approach. Wiley-VCH Verlag

GmbH & CO. KGaA; 2012.
[4] Tenek LH, Henneke II EG, Gunzburger MD. Vibration of delaminated composite plates and some applications to non-destructive testing. Compos Struct 1993;23:253–62.
[5] Phan TS, Dulieu-Barton JM, Temarel P. Thermoelastic stress analysis of structures under natural vibrations. Exp Mech 2006;46:463–72.
[6] Dulieu-Barton JM, Fruehmann RK, Quinn S. A full-field stress based damage assessment approach for in-situ inspection of composite structures. Key Eng Mater 2013;569:3–10.
[7] Fruehmann RK, Crump DA, Dulieu-Barton JM. Characterization of an infrared detector for high frame rate thermography. Meas Sci Technol 2013;24:1–12.
[8] Robinson AF, Dulieu-Barton JM, Quinn S, Burguete RL. Paint coating characterization for thermoelastic stress analysis of metallic materials. Meas Sci Technol 2010;21:1–11.
[9] Fruehmann RK, Dulieu-Barton JM, Quinn S, Peton-Walter J, Mousty PAN. The application of thermoelastic stress analysis to full-scale aerospace structures. Modern practice in stress and vibration 2012, Journal of Physics: Conference Series; 2012.
[10] ThyssenKrupp Materials International. Material data sheet ASTM A53; 2011.
[11] Sakagami T, Izumi Y, Mori N, Kubo S. Development of self-reference lock-in thermography and its application to remote nondestructive inspection of fatigue cracks in steel bridges. In: Proceedings of 10th international conference on quantitative infrared thermography, (Quebec, Canada); 2010.